Magnetosphere-ionosphere coupling at Jupiter:
Modeling the effects of temporal and local time variability

The goal of the proposed work is to quantify how magnetosphere-ionosphere coupling at Jupiter is affected by 1) local time asymmetries in the magnetosphere and 2) temporal variability related to the internal mass loading from Io and external forcing from the solar wind. In order to achieve this goal, we will combine data analysis from the Galileo spacecraft and the Hubble Space Telescope with computational models. The results of this work will improve our understanding of spatial and temporal variability in the brightness and location of Jupiter's main emission, which has implications for magnetosphere-ionosphere coupling in other rotation-dominated planetary systems.

1. Introduction

Auroral emissions are observed on planets and moons throughout the solar system. As a visible manifestation of magnetosphere-ionosphere (M-I) coupling, auroral emissions provide an excellent method for remotely sensing a planet's local magnetic field and plasma environment. Jupiter's UV auroral emissions, produced by excitation of atmospheric H_2 and H by precipitating electrons, are the brightest in the solar system at more than 10^{14} Watts (e.g. Bhardwaj and Gladstone, 2000), due largely to Jupiter's intense planetary magnetic field, the strongest in the solar system, and planetary rotation, the fastest in the solar system.

From equator to pole, Jupiter's UV auroral emissions consist of: satellite footprints, bright patches at the ionospheric end of field lines linked to the Galilean moons; a main oval emission; and the highly variable polar emissions, which include patchy emissions, flares, and a dark region, located interior to the main emission. The main emission falls in a relatively constant, narrow (1º-3º latitudinal width) band that is fixed with respect to System-III longitude (Grodent et al., 2003). In the northern hemisphere, the main emissions are not actually shaped like an oval, but display a kidney bean shape due to a magnetic anomaly; this shape can be seen in **Figure 1**, which is a polar projection of the UV auroral emissions in the northern hemisphere.

The Jovian main auroral emissions are not believed to be associated with magnetospheric interaction with the solar wind, as at the Earth, but instead with the breakdown of plasma corotation in the middle magnetosphere (Cowley and Bunce, 2001; Hill, 2001). Plasma from the Io torus diffuses radially outward through flux tube interchange, and must decrease its angular velocity in order to conserve angular momentum. Because the field is frozen into the flow, field

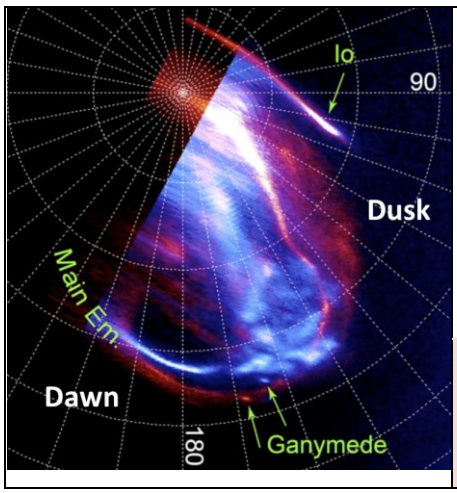

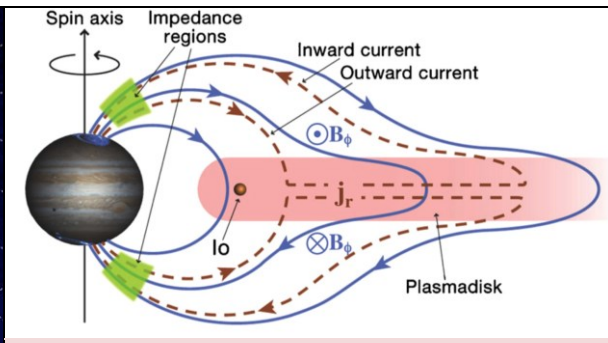

Figure 1. (left) HST images of Jupiter's aurora from 2000 (red) and 2005 (blue). From Grodent et al (2008). **(right, top)** Illustration of the current system (red dashed lines), driven by outward radial transport of Iogenic plasma, that produces the main emission. Blue solid lines are magnetic field lines. From Bagenal (2007).

lines in the magnetosphere are swept back azimuthally as the plasma's angular velocity decreases. A corotation enforcement current (CEC) system develops, illustrated in **Figure 1**, which features 1) an upward-directed (out of the ionosphere) field-aligned current that carries downgoing electrons that produce the main auroral emission, 2) an outward field-perpendicular radial current in the middle magnetosphere that provides a **j**×**B** force to accelerate plasma azimuthally back towards corotation, and 3) a return downward-directed (into the ionosphere) field-aligned current associated with upgoing electrons and hence no auroral emission. The ionospheric position of these CECs, and therefore the main auroral emission, depends on factors like the ionospheric conductivity, magnetic field configuration, and mass outflow rate of Iogenic plasma. Theoretical calculations suggest that the upward (out of the ionosphere) field-aligned currents associated with the breakdown of corotation are strongest at ~30 R_J radial distance in the equatorial magnetosphere (e.g. Cowley and Bunce, 2001; Hill, 2001; Nichols, 2011).

The brightness and position of the main auroral emission are influenced by both spatial and temporal variations in the M-I coupling system. Observations from the Galileo spacecraft show significant local time asymmetries in plasma flows, the ring current, and the configuration of the magnetic field in the magnetosphere (e.g. Krupp et al., 2001; Kivelson and Khurana, 2002; Khurana, 2001, 2004). These local time asymmetries can affect the M-I coupling system, leading to local time asymmetries in the main emission brightness or the radial distance in the magnetosphere to which the main emission maps. For example, as shown in **Figure 1**, there are morphological variations in the main oval as a function of local time: the dawn side portion forms a narrow arc, the post-noon portion consists of auroral patches, and the dusk portion is more broad and less discrete than the dawn emission (e.g. Grodent et al., 2003). Bonfond et al. (2015) reported that the main emission is ~1-3 times brighter near dusk than near dawn, and qualtitatively suggested that this is due to a partial ring current in the nightside magnetosphere (Khurana, 2001). The main emission also features a discontinuity, where the brightness is ~10% of typical values, that consistently maps to the pre-noon local time sector, where magnetic field measurements suggest that the field-aligned current reverses direction and flows downward into the ionosphere (Radioti et al., 2008; Khurana, 2001). Additionally, the reference main oval from Nichols et al. (2009) maps to significantly smaller magnetospheric radial distances near dawn (~20-30 R_J) than near dusk (~50-60 R_J) (e.g. Vogt et al., 2011, 2015).

<u>There have been relatively few theoretical or modeling studies of how magnetospheric local time asymmetries influence M-I coupling at Jupiter</u>. Instead, most studies assume complete azimuthal symmetry in the magnetic field and plasma properties (e.g. Cowley and Bunce, 2001; Nichols, 2011), which greatly simplifies the equations governing M-I coupling but neglects important local time asymmetries. An important exception is the work of Ray et al. (2014), which took a data-derived model for $B_N(r,LT)$ at one hour local time increments and applied it to a 1-D model of M-I coupling at Jupiter. (B_N is similar to B_θ, the meridional component of the magnetic field in spherical coordinates.) This model calculates the intensity and location of field-aligned currents and the plasma angular velocity in the magnetosphere. The results of Ray et al. (2014), shown in **Figure 2**, suggest that the local time asymmetries in the magnetic field resulted in: 1) strongest auroral currents in the dawn local time region, 2) weakest field-aligned currents in the noon-dusk sector, which should lead to dim auroral emissions in this region, 3) faster azimuthal plasma velocity at dusk than at dawn, and 4) a ~6º difference in the main emission colatitude at dawn vs. dusk. The results disagree somewhat with observations: the minimum in the auroral and radial currents are observed closer to dawn than predicted by the model, and Galileo energetic particle observations show that the azimuthal plasma velocity is fastest near

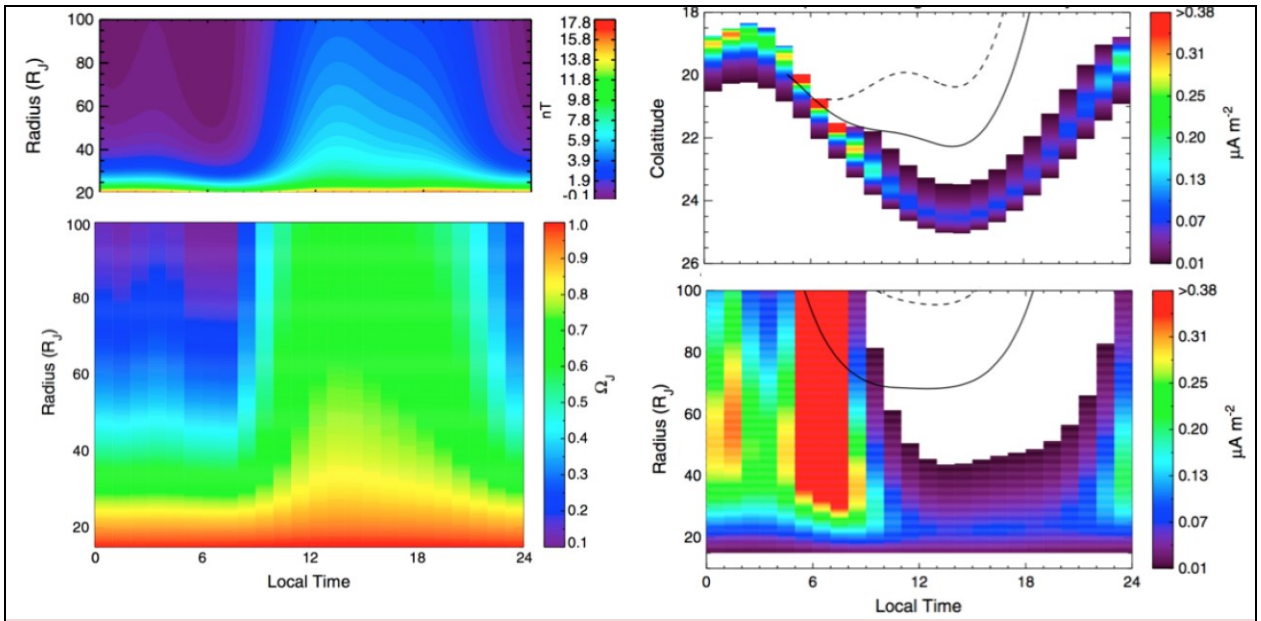

Figure 2. Results of a local time dependent M-I coupling model, reproduced from Ray et al. (2014). The magnetic field in the top left panel is the model input and the remaining quantities are model outputs, which all depend on local time (LT). **(top left)** The equatorial radial distance and local time dependence of a magnetic field component similar to B_θ. **(bottom left)** Plasma angular velocity in the magnetosphere as a function of radial distance and LT. **(top right)** Ionospheric field-aligned current density as a function of colatitude and LT. The colored areas show locations of expected auroral emissions (where the field-aligned current density is larger than the electron thermal current density). **(bottom right)** Ionospheric field-aligned current density mapped to the magnetosphere, as a function of radial distance and LT.

dawn, not dusk. Therefore, it remains unclear how local time asymmetries in the magnetic field and plasma properties at Jupiter lead to differences of ~30 R_J in the mapped location of the main emission at dawn versus dusk (Vogt et al., 2011, 2015). Though the Ray et al. model included local time asymmetries in the equatorial magnetic field it made several simplifying assumptions, including azimuthal symmetry in the Io mass outflow rate and constant Pedersen conductance, and neglected the magnetic field "bendback", which describes how a magnetic field line is swept out of the meridional plane. The magnetic field bendback varies with local time (e.g. Khurana, 2001), with field lines being most strongly bent back near dawn and bent forward in the dusk sector, as shown in **Figure 3**. This should be reflected in the local time dependence of the plasma angular velocity (if the field is frozen into the flow) and radial component of the CEC system. Ray et al. (2014) concluded that "(f)uture studies of local time variation in the M-I current system should consider the bendback of the planetary magnetic field".

In addition to varying with local time, the main emission also varies temporally, with shifts in the main emission of several degrees of latitude on time scales from months to years. One such example is shown in the left panel of **Figure 1**, which shows a superposition of HST observations from December 2000 (red) and April 2005 (blue) from Grodent et al. (2008). These images were taken with similar viewing geometries but the main emission and Ganymede footprint are shifted by ~2-3º latitude from one image to the other. Similarly, HST images show a steady ~2º expansion of the main emission from February to June 2007, although the Ganymede footprint in this example did not shift in latitude (Bonfond et al., 2012). Shifts in the

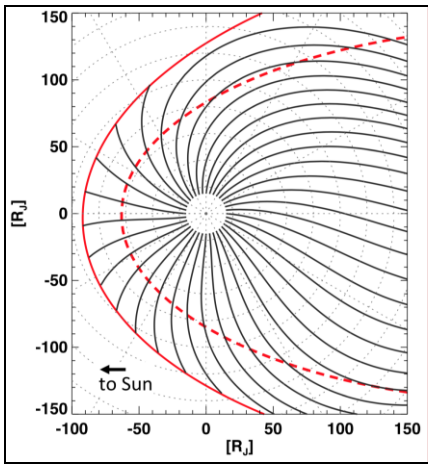

Figure 3. Field bendback model, projected onto the equatorial plane, based on fits to magnetic field data (from Vogt et al., 2011). The magnetic field is bent back out of a meridian plane at dawn and swept forward and dusk.

main emission position can be caused by changes in the magnetospheric field configuration, which alter the ionospheric mapping of field lines at a fixed distance in the equatorial plane and must also shift the Ganymede footprint, since the satellite footprint must be linked to Ganymede's orbital radial distance of 15 R_J. However, shifts in the main emission without a corresponding change in the Ganymede footprint, like that reported in Bonfond et al. (2012), must be caused by changes in parts of the M-I coupling system other than the field geometry.

Theoretical calculations and modeling work have been used to study how temporal changes in parts of the M-I coupling system, including the mass outflow rate of Iogenic plasma, ionospheric Pedersen conductivity, and plasma properties like density and angular velocity, can affect the position of the main emission (e.g. Cowley and Bunce, 2003a, 2003b; Nichols, 2011; Nichols et al., 2015). Such calculations can be particularly useful for understanding how the M-I coupling system is affected by changes in quantities that are difficult to measure, like the mass loading rate from Io and the Pedersen conductivity. The M-I coupling system also depends on the configuration of the magnetic field in the magnetosphere, which can vary in response to internal (e.g. enhanced mass loading) and external (e.g. solar wind dynamic pressure) drivers affecting the M-I coupling process. Measurements of the temporal changes in the magnetic field are readily available but have not yet been accurately incorporated into M-I coupling model calculations to quantify how much the main auroral emission should shift in response to temporal changes in the magnetic field.

We propose to quantify local time asymmetries and temporal variability in the magnetic field measurements from Jupiter's magnetosphere and to use this information in calculations and models to determine their effects on the M-I coupling system at Jupiter. Our calculations will broadly follow the approach of previous other studies that have quantified the M-I coupling system at Jupiter, but, crucially, will move beyond the assumption of complete azimuthal symmetry and will include the effects of the magnetic field asymmetries and temporal variability. Our work will answer the following questions:

- **How do local time asymmetries in Jupiter's magnetosphere affect the brightness and position of the main auroral emission?**
- **How does the magnetosphere-ionosphere coupling system at Jupiter change in time?**

We will quantify how local time asymmetries in Jupiter's magnetic field affect the brightness and position of Jupiter's main auroral emission, which will finally help us understand why the main emission maps to ~30 R_J near dawn and ~60 R_J near dusk. We will determine how temporal changes in the magnetic field lead to changes in Jupiter's M-I coupling system, which is a first step toward understanding the relative role of internal (changes in the mass loading rate from Io) and external (solar wind) drivers of auroral variability. We will compare the predicted auroral shifts to observations, particularly to HST observations concurrent with the Galileo data, which will further constrain estimates of variability in hard-to-measure quantities like the mass

loading rate and Pedersen conductivity. The results of this study will be timely, given that NASA's Juno mission is studying Jupiter's polar magnetosphere and aurora and has recently (Feb. 2017) completed its fourth perijove pass. By informing our understanding of M-I coupling at Jupiter, our work will also have implications for our understanding of M-I coupling in other rotation-dominated systems in our solar system, like Saturn, and potentially in exoplanetary systems (e.g. Nichols, 2011b, 2012).

2. Summary of proposed research

The proposed research consists of 3 tasks. **Task A** will establish global 2-dimensional fits, accounting for changes in radial distance and local time, to the magnetic field components in Jupiter's magnetosphere from magnetometer data near the jovigraphic equator. We will also use the magnetic field measurements to calculate a 2-D global fit to the height-integrated radial current flowing in the magnetosphere, which will be used to calculate ionospheric field-aligned currents that produce the main auroral emissions following the theoretical framework of Bunce and Cowley (2001). The 2-D fits to the magnetic field will also be used as input to a self-consistent magnetodisk model in **Task B** to study how the local time dependence of the magnetic field, established from Task A, will affect factors like the main emission mapping and magnetospheric plasma parameters. **Task C** will study how temporal variability observed in Galileo measurements of the magnetic field contributes to changes in the position of Jupiter's main auroral emission. Temporal variations in the magnetic field will be used as input to the calculations and models from Tasks A and B to predict how the main emission would shift in response, and the results will be compared to HST observations of the main emission variability.

2.1 Task A: Establishing global 2-dimensional functions for the magnetic field and currents

In this task we will analyze magnetometer data to establish 2-dimensional functional fits to the magnetic field components and currents flowing in the magnetosphere. Most M-I coupling studies used radial profiles of the magnetic field to calculate radial profiles of the plasma angular velocity and radial (in the magnetosphere) and colatitudinal (in the ionosphere) profiles of the parallel currents that drive the main emission. We propose to instead use a representation of the

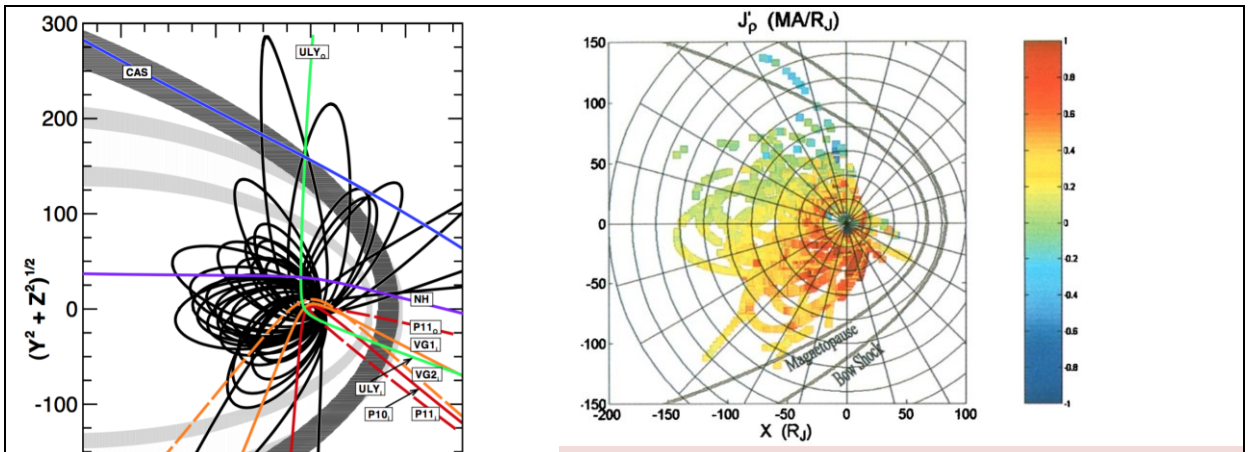

Figure 4. (left) Equatorial projections of spacecraft trajectories at Jupiter (Vogt, 2012). **(right)** The height-integrated radial current density in the equatorial plane (Khurana, 2001). The Sun is to the right.

equatorial magnetic field that is a function of both radial distance and local time, accounting for the magnetic field bendback, to establish how local time asymmetries in Jupiter's magnetic field influence M-I coupling at Jupiter and the position and brightness of the main auroral oval.

Magnetic field measurements are available in Jupiter's magnetosphere from the Pioneer 10, Pioneer 11, Voyager 1, Voyager 2, and Ulysses flybys of Jupiter, as well as from the Galileo orbiter (1996-2003). All data are available on the PDS. **Figure 4 (left)** shows the spacecraft trajectories in the equatorial plane (note that New Horizons, shown in purple, did not include a magnetometer and Cassini, shown in blue, stayed outside of the magnetosphere). The majority of data come from the Galileo orbiter, though the other spacecraft flybys are valuable because provide coverage in the dawn-noon local time sectors. Overall, the radial distance and local time coverage is sufficient to create 2-D functional fits to the equatorial magnetic field components.

Figures 4 (right) and 5 show that the magnetic field and currents derived from it display strong local time asymmetries (as well as an exponential falloff with radial distance), and that this spatial dependence can be well described with a 2-D functional fit. **Figure 4 (right)** shows the height-integrated radial current density in the equatorial plane, which is strongest in the dawn local time sector and weakest (and, at large R, reversed in sign) at dusk, as calculated by Khurana (2001) using magnetic field data. **Figure 5** shows an example 2-D fit in the equatorial plane to B_N, a component of the magnetic field that is similar to B_θ, the meridional component of the magnetic field in spherical coordinates, from Vogt et al. (2011). They assumed a functional form

$$B_N(R,\varphi) = A\,R^{(B+C\cos(\varphi-D))} + \left[E + F\cos(\varphi-G) + H\cos(2\times(\varphi-I)) + J\cos(3\times(\varphi-K))\right]\times e^{-R/150} \quad (1)$$

where R is the radial distance in R_J; φ is the local time, measured from midnight, in radians; and A, B, C, D, E, F, G, H, I, J, and K are constants determined by the fitting routine. Ray et al. (2014) used a slightly modified version of this function as input to their M-I coupling model.

<u>We propose to calculate similar 2-D fits to all of the available magnetic field data from Jupiter's magnetosphere and use these fits to study how M-I coupling currents at Jupiter are influenced by local time asymmetries in Jupiter's magnetic field.</u> Bunce and Cowley (2001) calculated the radial and azimuthal currents in the current sheet from Pioneer and Voyager flyby magnetic field data and used this to calculate the expected field-aligned current and radial profiles of the plasma angular velocity associated with M-I coupling. However, this study used a limited amount of data and therefore did not examine local time effects. Khurana (2001) calculated currents in the equatorial plane from the Galileo data (as shown in **Figure 4 (right)**), but only used data through the end of May 2000 so 7 Galileo orbits from mid-2000 to 2003 are missing, which would fill in the noon-dusk local time sector (see **Figure 4**), and did not apply

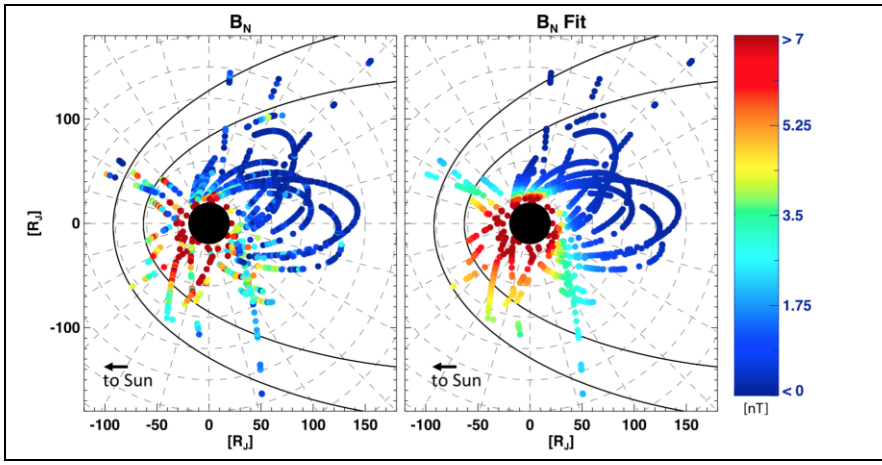

Figure 5. Data (left) and model fit to a 2-D function (right) of B_N in the equatorial plane in Jupiter's magnetosphere. B_N is similar to B_θ, the meridional component of the magnetic field in spherical coordinates. From Vogt et al. (2011)

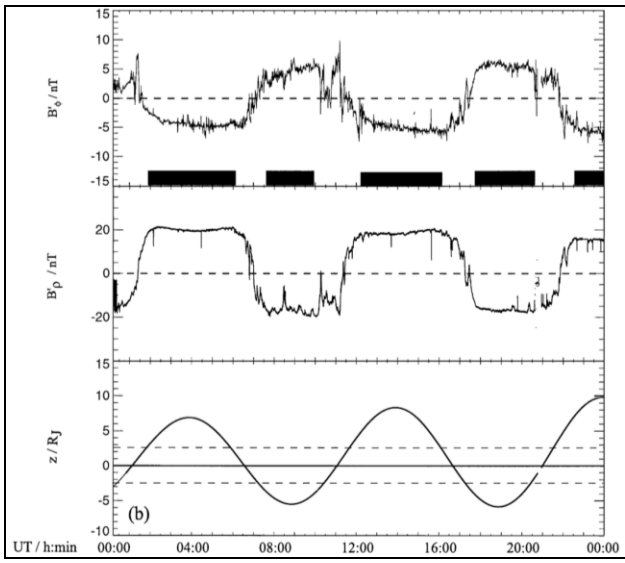

Figure 6. Time series of Voyager 2 perturbation magnetic field components, calculated by removing the planetary internal field from the observed magnetic field. (Top) Azimuthal external field $B_{\varphi,ext}$. (Middle) Radial external field $B_{R,ext}$. (Bottom) Vertical distance z from the current sheet. Black bars show times when the spacecraft was outside of the current sheet, as evidenced by the large radial field. Modified from Bunce and Cowley (2001).

these currents to the M-I coupling system. We will improve on these past studies by including all of the available data, which provides complete local time coverage.

Our work will be done in 3 steps. **Step 1** is to calculate 2-D fits to the magnetic field components B_ρ, B_φ, and B_z (in cylindrical coordinates) outside the current sheet. Most of the magnetic field data at Jupiter was obtained from spacecraft near the jovigraphic equator. Because of the ~10º dipole tilt the current sheet (located roughly in the magnetic equator) passes over the spacecraft every 5 hours (1 Jovian rotation period is roughly 10 hours). B_ρ and B_φ typically reverse sign during a current sheet crossing. **Figure 6** shows an example of this periodicity and how it can be used to identify magnetic field data from outside of the current sheet (thick black bars). Current sheet intervals can be identified visually or automatically by imposing some quantitative criteria (e.g. the spacecraft is typically in the lobe when $|B_\rho|/|\mathbf{B}|$ is greater than some threshold value). We will fit the measured B_ρ, B_φ, and B_z to functions that include an exponential radial falloff and include a sinusoidal dependence on local time, similar to equation 1. Following previous studies (e.g., Caudal, 1986; Khurana, 1997), we will select the magnetic field functional forms so that the magnetic field can be expressed in terms of two scalar stream functions or Euler potentials, α and β, which is possible because **B** is divergenceless, as follows

$$\vec{B} = \nabla\alpha \times \nabla\beta \quad (2).$$

In this case, the magnetic field in cylindrical coordinates (ρ,φ,z) is given by

$$\vec{B} = \frac{1}{\rho}\left(\frac{\partial\alpha}{\partial\varphi}\frac{\partial\beta}{\partial z} - \frac{\partial\alpha}{\partial z}\frac{\partial\beta}{\partial\varphi}\right)\hat{\rho} + \left(\frac{\partial\alpha}{\partial z}\frac{\partial\beta}{\partial\rho} - \frac{\partial\alpha}{\partial\rho}\frac{\partial\beta}{\partial z}\right)\hat{\varphi} + \frac{1}{\rho}\left(\frac{\partial\alpha}{\partial\rho}\frac{\partial\beta}{\partial\varphi} - \frac{\partial\alpha}{\partial\varphi}\frac{\partial\beta}{\partial\rho}\right)\hat{z} \qquad (3).$$

Step 2 is to calculate currents from the magnetic field fits using Ampere's law, as was successfully done Bunce and Cowley (2001) and Khurana (2001). The observed magnetic field **B** is the sum of the internal planetary field ($\mathbf{B_{int}}$) and the external or perturbation field ($\mathbf{B_{ext}}$) due to currents flowing in the magnetosphere. These currents include the magnetopause current, partial ring current, neutral sheet current, and corotation enforcement currents (see review by Khurana et al., 2004). They have the effect of stretching the dipole magnetic field radially and out of a meridian plane (bendback or sweep forward). We will calculate the external field by subtracting the internal field, given by a model (e.g. VIP4, Connerney et al. 1998, or VIPAL, Hess et al., 2011), from the observed field. We will then use the external field to calculate the magnitude and direction of the currents with Ampere's law, which in cylindrical coordinates (ρ,φ,z) is given by

$$\nabla \times \vec{B}_{ext} = \mu_0 \vec{j} = \left(\frac{1}{\rho} \frac{\partial B_{z,ext}}{\partial \varphi} - \frac{\partial B_{\varphi,ext}}{\partial z} \right) \hat{\rho} + \left(\frac{\partial B_{\rho,ext}}{\partial z} - \frac{\partial B_{z,ext}}{\partial \rho} \right) \hat{\varphi} + \frac{1}{\rho} \left(\frac{\partial \left(\rho B_{\varphi,ext} \right)}{\partial \rho} - \frac{\partial B_{\rho,ext}}{\partial \varphi} \right) \hat{z} \quad (4),$$

where j is current density. Because the spacecraft position moves in time the partial derivatives of the magnetic field components cannot be calculated directly from the data, but simplifying assumptions can be made. For example, near the equatorial plane B_ρ varies more slowly with ρ and φ than with z so B_ρ can be treated as a function of z alone, which simplifies the calculation of **j** (see Bunce and Cowley, 2001 and Khurana, 2001 for a complete discussion). Integrating j_ρ over the current sheet height then gives the integrated radial current intensity i_ρ:

$$i_\rho = \frac{2}{\mu_0} \left[\frac{D}{\rho} \frac{\partial B_{z,ext}}{\partial \varphi} - B_{\varphi,ext} \right] \approx -\frac{2}{\mu_0} B_{\varphi,ext} \quad (5),$$

where D is the current sheet half-thickness (Bunce and Cowley, 2001, equations 3 and 6). The azimuthal current is (Bunce and Cowley, 2001, equation 8):

$$i_\varphi = 2B_{\rho,ext} / \mu_0 \quad (6).$$

Note that equations 5 and 6 account for local time variations in the magnetic field bendback, which depends on the ratio of B_φ to B_ρ.

<u>Step 3</u> calculates radial profiles of the plasma angular velocity and auroral currents from the currents calculated in step 2. For a complete derivation of the following equations and their successful application we refer the reader to Bunce and Cowley (2001) and the other references given. The radial current associated with the M-I coupling circuit, $\rho i_{\rho MI}$, is given by

$$\rho i_{\rho MI} = \rho i_\rho - \rho i_{\rho CS} \quad (7),$$

where i_ρ comes from equation 5 above and $i_{\rho CS}$ is defined as the radial current that combines with i_φ (equation 6) to make the current divergenceless (see Bunce and Cowley, 2001, equations 13-18). We can then calculate the plasma angular velocity ω

$$\frac{\omega}{\Omega_J} \approx 1 - \frac{\rho i_{\rho MI}}{4 \Sigma_p^* \Omega_J F} \quad (8),$$

where Σ_P^* is the effective Pedersen conductivity, Ω_J is the planetary rotation period, and F is the flux function (Bunce and Cowley, 2001, equation 34). The flux function is the magnetic flux per unit azimuth threading the equatorial plane or the ionosphere. Equating the equatorial and ionospheric flux functions provides a way to link a radial distance in the magnetosphere to an ionospheric colatitude. For a non-axisymmetric field the equatorial flux function F_e is given by

$$F_e(\rho, \varphi) = \int_\rho^\infty \rho B_z(\rho, \varphi, z = 0) \; d\rho \quad (9),$$

(e.g. Ray et al. (2014), equation 7). We will follow previous studies (e.g. Cowley and Bunce, 2001; Ray et al., 2014) in assuming the ionospheric magnetic field is given by a simple axisymmetric dipole field; while this does not represent a realistic planetary magnetic field it allows us to focus on the effects of magnetospheric local time asymmetries. The ionospheric flux function F_i is therefore

$$F_i(\theta_i) = B_J R_J^2 \sin^2 \theta_i \quad (10),$$

where B_J is the equatorial magnetic field strength and θ_i is the ionospheric colatitude (e.g. Cowley and Bunce, 2001, eq. 3). The field-aligned current density $j_{//}$ can then be calculated by

$$\frac{j_{//}}{B} = -2 \frac{d}{dF} \left(\Sigma_P^* \left(\Omega_J - \omega \right) F \right) \quad (11)$$

(Bunce and Cowley, 2001, equation 32). The field-aligned current in the equatorial plane, which gives the magnetospheric mapping of the main emission, is calculated by using F_e in equation 11, while the field-aligned current in the ionosphere, which gives the ionospheric position of the main emission, is calculated by using F_i in equation 11.

The outputs of the work in this task will be: 1) 2-D (R, LT) functional fits to the magnetic field in Jupiter's magnetosphere, from which we can derive 2-D functions of magnetospheric currents and 2) 2-D (R, LT) functions of the plasma angular velocity ω (equation 8) and field-aligned currents in the magnetosphere and ionosphere (equation 11), quantities which previously have typically been expressed as radial profiles without considering the dependence on local time. We will produce plots like **Figure 4 (right)** and **Figure 5**, but for all components of the magnetic field and currents, and plots like **Figure 2** but we will account for local time asymmetries in all magnetic field components (and the magnetic field bendback), not just B_z. The physical significance of these results is that we will have quantified how local time asymmetries in Jupiter's magnetosphere affect the M-I coupling system that drives Jupiter's main emission. Using these results we will make predictions of how the local time dependence of the magnetic field should affect the main emission brightness (from the magnitude of the field-aligned currents) and position (from the radial/colatitudinal profile of the field-aligned currents). We will also test the qualitative prediction from Bonfond et al. (2015) that dawn-dusk asymmetries in the auroral brightness can be explained by the nightside partial ring current described by Khurana (2001). We will publish a paper describing our results in a peer-reviewed journal.

Finally, we note that this study can be slightly scaled back, but still produce scientifically significant and publishable results, in the unlikely event of unforeseen difficulties. For example, we expect to be able to successfully derive 2-D functions of the magnetic field, and derive 2-D functions for the magnetospheric currents, based on our previous experience fitting B_N (Vogt et al., 2011). However, if we cannot find a suitable 2-D fit or if we encounter problems applying the above equations to a 2-D field model, we can take data from a few representative local time ranges (e.g., 00:00-02:00, 06:00-08:00, 12:00-14:00, and 18:00-20:00) and fit simple radial fall offs to all 3 components of the magnetic field at these local times. We can then follow the analysis of Bunce and Cowley (2001) and obtain radial profiles of the plasma angular velocity and auroral currents that apply to each local time, which would still provide valuable insight into how Jupiter's M-I coupling system changes with local time.

2.2 Task B: Employing a self-consistent magnetodisk model to study local time effects

In this task we will use the 2-D fits to the magnetic field obtained from Task A as input to a self-consistent magnetodisk model. Using this model allows us to study how the local time dependence of Jupiter's magnetic field affects the main emission mapping and plasma angular velocity, like the theoretical calculation in Task A, but it also allows us to 1) model how changes in the mass loading rate from Io and the Pedersen conductivity, two quantities that are poorly constrained by measurements, affect the M-I coupling system at different local times, and 2) self-consistently consider how the local time effects in the magnetic field affect plasma pressure throughout the magnetosphere. This first point is important for interpretation of temporal variability in HST images or upcoming Juno Ultraviolet Spectrograph (UVS) observations of Jupiter's aurora. The second point is important in part because an eventual next step in modeling the local time asymmetries in M-I coupling at Jupiter will be to consider local time variability in the plasma mass outflow rate $\dot{M}$. The plasma mass outflow rate is related to the rate of mass loading from Io and the magnetospheric plasma density (e.g. Bagenal and Delamere, 2011),

which we will obtain from this model and is dependent on local time. We do not propose to consider local time variability in the plasma mass outflow rate here, choosing instead to focus on effects of local time asymmetries in the magnetic field. However, we note that our work will provide an important first step toward including local time asymmetries in the plasma mass outflow rate and fully modeling the local time variability of M-I coupling at Jupiter.

We will follow the general approach of the Nichols (2011) self-consistent magnetodisk model but will modify the model to take the magnetic field as an input, not an output, and will include azimuthal asymmetries. We begin in section 2.2.1 by reviewing the Nichols (2011) model, then in section 2.2.2 we discuss modifications and expected results and significance.

2.2.1 Magnetodisk model of Nichols (2011)

The Nichols (2011) magnetodisk model takes as its inputs the density and temperature of plasma in Jupiter's magnetodisk, the mass loading rate from Io, and the effective Pedersen conductance. The model applies an iterative process to solve for a self-consistent magnetic field configuration and plasma angular velocity. It uses the equations that describe Jupiter's M-I coupling current system to calculate a plasma angular velocity that is consistent with an initial (dipole) magnetic field configuration, then calculates the currents associated with that plasma angular velocity via the momentum equation, and finally identifies a new magnetic field configuration that is consistent with those currents via Ampere's law. The process repeats, calculating the plasma angular velocity from the new magnetic field configuration instead of the initial dipole, and continues until the initial and final magnetic field values agree to within 0.5%. Each model run takes about 10-60 minutes on a standard desktop computer. The Nichols (2011) model is based on an earlier model by Caudal (1986) that used a fixed plasma angular velocity profile that was consistent with a dipole magnetic field.

Here we describe the equations used in the model in more detail. The M-I coupling equation that calculates the plasma angular velocity from the magnetic field is called the Hill-Pontius differential equation for the plasma angular velocity ω:

$$\frac{\rho_e}{2}\frac{d}{d\rho_e}\left(\frac{\omega}{\Omega_J}\right)+\left(\frac{\omega}{\Omega_J}\right)=\frac{4\pi\Sigma_P^* F_e\left|B_{ze}\right|}{\dot{M}}\left(1-\frac{\omega}{\Omega_J}\right), \quad (12)$$

where ρ_e is equatorial radial distance, Ω_J is Jupiter's planetary rotation period, Σ_p^* is the effective Pedersen conductance, F_e is the equatorial flux function (equation 9), B_{ze} is the z component of the magnetic field at the equator, and $\dot{M}$ is the plasma mass outflow rate (Nichols, 2011, eq. 3; see also Hill, 1979, 2001; Pontius, 1997; and Cowley et al., 2002). This equation assumes the outward flow of plasma through the system is axially symmetric.

Following Caudal (1986), Nichols (2011) represented the magnetic field **B** using two scalar stream functions α and β following equation 2 above, and assumed an axisymmetric field with $B_\varphi = 0$, which is satisfied if $\alpha = \alpha(r,z)$ and $\beta = a\varphi$ for some constant a. The magnetic field in cylindrical coordinates (ρ,φ,z) is then given by equation 3 above, which is greatly simplified by the assumption of axisymmetry.

The momentum equation relates the plasma angular velocity ω and plasma pressure P to currents **j**:

$$\vec{j}\times\vec{B}=\nabla P-d\omega^2\rho\hat{\rho} \quad (13),$$

where d is the plasma mass density (Nichols, 2011, eq. 11). The plasma pressure is given by the ideal gas law and depends on both the plasma temperature and plasma density, which for the cold (~100 eV) plasma depends on ω because the plasma is centrifugally confined to the equator

(see Nichols, 2011, eqs. 16-19). For the hot plasma (~30 keV) the second term on the right hand side of equation 5 can be neglected because it is dominated by the pressure term. We note that therefore the magnetodisk model calculations effectively only consider the cold plasma pressure, since the hot plasma is unaffected by the plasma angular velocity.

Finally, Ampere's law (equation 4 above) relates the currents from the momentum equation (eq. 13) to the magnetic field. Under the assumption of axisymmetry and $B_\varphi = 0$, Ampere's law reduces to only the azimuthal (φ) component, with $j_r = j_z = 0$, and only the radial component of $\mathbf{j}\times\mathbf{B}$ is nonzero.

Together, equations 4, 12, and 13 form the basis of a general self-consistent magnetodisk model. Caudal (1986) showed that, under the assumption of an axially symmetric magnetic field, one can derive the following differential equation that relates ω and the cold plasma pressure P_c to the magnetic field stream function α:

$$\frac{\partial^2\alpha}{\partial r^2}+\left(\frac{1-x^2}{r^2}\right)\frac{\partial^2\alpha}{\partial x^2}=\mu_0\left(\frac{\rho}{R_J}\right)^2\exp\left(\frac{\omega^2 m\left(\rho^2-\rho_0^2\right)}{4kT_c}\right)\left[\frac{dP_{c,0}}{d\alpha}+\frac{\omega^2 m\left(P_{c,0}R_J\right)}{2kT_c\left|B_{z0}\right|}\right] \quad (14),$$

where $x = \cos(\theta)$, where r and θ are the radius and inclination in spherical coordinates; R_J is the Jovian radius; m is the ion mass; k is Boltzmann's constant; T_c is the cold plasma temperature; and the '0' subscripts (e.g. ρ_0) indicate values at the equator. The left hand side of equation 14 comes from expressing $\nabla\times\vec{B}$ from Ampere's law in terms of the stream function α and the right hand side of equation 14 comes from the right hand side of equation 13. In summary, the Nichols (2011) model solves equation 12 for the plasma angular velocity ω that is consistent with the input magnetic field, then uses that ω in equation 14 to identify the corresponding stream functions (from which the output magnetic field can be calculated using equation 3); the process repeats iteratively until the input and output magnetic field agree to within 0.5%.

Nichols (2011) used the model to calculate the magnetic field and plasma angular velocity for different values of Σ_p^* and $\dot{M}$. **Figure 7** shows model results for two different values of $\Sigma_p^*/\dot{M}$. Nichols (2011) also calculated radial profiles of the azimuthally integrated equatorial radial current and field-aligned current density at the top of the ionosphere to show how relative changes in Σ_p^* and $\dot{M}$ could shift the ionospheric position of main auroral emission.

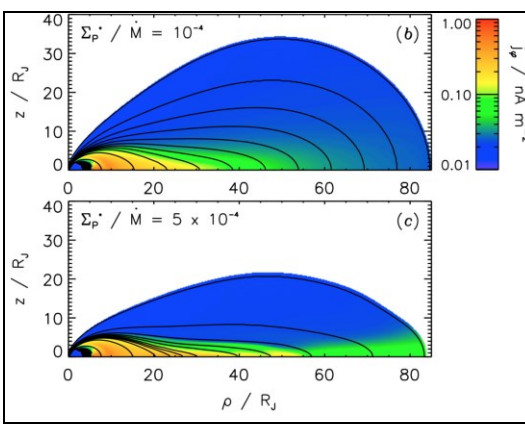

Figure 7. Nichols (2011) model results for different values of $\Sigma_p^*/\dot{M}$, 10^{-4} (top) and 5×10^{-4} (bottom) mho s kg^{-1}. Black lines show magnetic field lines and color indicates azimuthal current density.

2.2.2 Modifications to the Nichols (2011) self-consistent magnetodisk model

We will follow the general approach of the Nichols (2011) magnetodisk model, with two major changes. <u>The first modification</u> to the Nichols (2011) model is that we will use a fixed magnetic field configuration, taking into account local time asymmetries as calculated in Task A, as input to the model and will solve for the plasma angular velocity and plasma pressure (which was provided as fixed input to the Nichols (2011) model). The magnetic field will be represented by the 2-D fits obtained in Task A. Therefore <u>the second modification</u> to the Nichols (2011) model is that we will no longer assume an axisymmetric magnetic field. These modifications

mean that equation 14 can no longer be used as a solution to equation 13, though we can still use equation 12 under the assumption that the mass outflow rate is axially symmetric.

Equation 14 is valid only under the assumption of axisymmetry, and specifically for $B_\varphi = 0$, and comes from applying **j** from Ampere's law (which is nonzero in the φ component only) to equation 13, which is greatly simplified because the radial component only of **j**×**B** is nonzero. Since our calculation will take into account azimuthal (local time) variations, all three components of **j** will be nonzero and can be calculated from Ampere's law (equation 4). Equation 13 then becomes (broken down into components):

$$\left(\vec{j}\times\vec{B}\right)_\rho = j_\varphi B_z - j_z B_\varphi = \frac{\partial P}{\partial \rho} - d\omega^2\rho \qquad \left(\vec{j}\times\vec{B}\right)_\varphi = j_z B_\rho - j_\rho B_z = \frac{\partial P}{\partial \varphi}$$

$$\left(\vec{j}\times\vec{B}\right)_z = j_\rho B_\varphi - j_\varphi B_\rho = \frac{\partial P}{\partial z} \qquad (15).$$

Though solving these equations is more complicated than solving equation 14, all quantities are known except P, and we can solve the equations analytically or numerically. We will follow Nichols (2011) eqs. 16-19, and assume the pressure is given by:

$$P = {2NkT_c}/{V} = 2NkT_c \Bigg/ \left(\int \exp\left(\frac{\omega^2 m\left(\rho^2 - \rho_0^2\right)}{4kT_c} \right) \frac{1}{B} ds \right) \qquad (16),$$

where N is the number of ions per Weber, V is the volume of the unit flux tube, and s is distance along the field line. Because ω and B are functions of local time N and T_c will be also.

<u>The outputs of the work in this task are</u> model calculations of how the plasma angular velocity and pressure (including density and temperature) vary with radial distance and local time in Jupiter's magnetosphere, consistent with the spatial dependence of the magnetic field as determined from Task A. We will produce model results for a range of values of $\Sigma_p^* / \dot{M}$, and will calculate the expected field-aligned currents for different values of $\Sigma_p^* / \dot{M}$. <u>The physical significance of these results</u> is that, as in Task A, we will have quantified how local time asymmetries in Jupiter's magnetosphere affect the M-I coupling system that drives Jupiter's main emission, but we will also have quantified the effects on plasma pressure throughout the magnetosphere. Finally, we will have modeled how changes in the mass loading rate from Io and the Pedersen conductivity affect the M-I coupling system at different local times. We will publish the results of this task as a paper in a peer-reviewed journal.

Finally, we note that, as in Task A, this study could be scaled back in the event of unforeseen difficulties performing any of the above calculations using the full 2-D functions of the magnetic field. In that case we would use simple radial fall offs for the magnetic field from a few representative local time ranges and obtain axisymmetric model results that apply to the 1-D magnetic field from each local time sector.

2.3 Task C: Modeling time variability in Jupiter's M-I coupling system

The magnetic field in Jupiter's magnetosphere displays both temporal and spatial variability. For example, the left panel of **Figure 5** shows that the magnetic field varies in a given (R, LT) location. In Tasks A and B we will have established how local time variability in the magnetic field affects the M-I coupling current system at Jupiter and the brightness and position of the main auroral emission. In this task we consider the effects of temporal variability in Jupiter's magnetic field, which can be driven internally (i.e. by changes to the rate at which volcanic activity from Io adds plasma to the magnetosphere) or externally (i.e. by the arrival of a

solar wind compression). For example, **Figure 8 (left)** shows how the B_z component of the magnetic field, measured by Galileo in the magnetosphere, increased in response to a solar wind compression measured by Cassini when it was upstream of Jupiter. Previous studies have considered the effects of temporal changes in Jupiter's magnetospheric field on the M-I coupling system (e.g. Cowley and Bunce, 2003a, 2003b; Southwood and Kivelson, 2001). Nichols (2011) used their magnetodisk model to consider the effect of temporal changes in the ratio of $\Sigma_p^* / \dot{M}$ (**Figure 7**) but did not discuss how the modeled variability of the magnetic field compared to what has been observed in spacecraft data.

To date, no study has yet used quantified the *measured* temporal changes in Jupiter's magnetic field and used the *measured* variability to calculate the expected changes in the M-I coupling system; we propose to do so in this task. This would represent an important contribution because 1) it can be used to constrain temporal variability in other quantities that are difficult to measure, like the mass loading rate from Io or the Pedersen conductivity, and 2) temporal changes in the magnetic field may themselves vary spatially, so performing the calculation with a realistic magnetic field will provide better insight into the expected auroral changes. As an example, one might expect that the effects of a solar wind compression would be most noticeable in the middle-outer magnetosphere and at dayside local times, with relatively little variability on the nightside or at distances inside of ~20 R_J.

Our approach will be to follow the procedure outlined in Task A but to obtain two 2-D fits to the magnetic field data representing temporal extremes for a "weak" and "strong" external magnetic field. For example, the 2-D fits from Task A will have been calculated using all data averaged over all internal and external conditions, which we will call the "average" fit. The "weak" ("strong") fit could be then calculated using only data that fall below (above) the "average" fit. Another option would be to use a model to predict the solar wind conditions upstream of Jupiter (e.g. Tao et al., 2005; Zieger and Hansen, 2008) and obtain "weak" and "strong" fits by including only data when the magnetosphere is likely to be in its expanded or compressed states, respectively, as predicted by the upstream solar wind dynamic pressure. As part of PI Vogt's NSF fellowship we have identified times when upstream solar wind models predict the magnetosphere is compressed or expanded, as shown in **Figure 8 (right)**, which could be used to construct the "weak" and "strong" 2-D magnetic field fits. Though the solar wind models are subject to error we are relatively confident in our analysis because the spacecraft was always located within the Joy et al. (2002) compressed magnetopause boundary when the solar wind models predicted a "compressed" magnetosphere. This also shows that the amount of data and its spatial coverage is sufficient to obtain two separate 2-D fits.

After obtaining two magnetic field fits representing two temporal extremes for the magnetic field configuration in Jupiter's magnetosphere we will then follow the work plan described in Tasks A and B, but starting from the "weak" and "strong" magnetic field fits instead of the "average" fit. We will calculate the plasma angular velocity and field-aligned currents necessary that is consistent with each of the "weak" and "strong" magnetic field fits. This will provide a quantitative prediction of the temporal variability in the main emission position and brightness that is consistent with the temporal variability in the magnetic field.

We will then compare the predicted auroral variability to that observed in HST images. This will help constrain estimates of the hard-to-measure quantities Σ_p^* and $\dot{M}$ and their temporal variability. HST auroral observations are available from 11 dates that overlap with the Galileo data, from 1996 through the end of 2002. HST images from these dates show that the main emission shifts by about ~2.5 degrees latitudinally during the Galileo era, similar to the

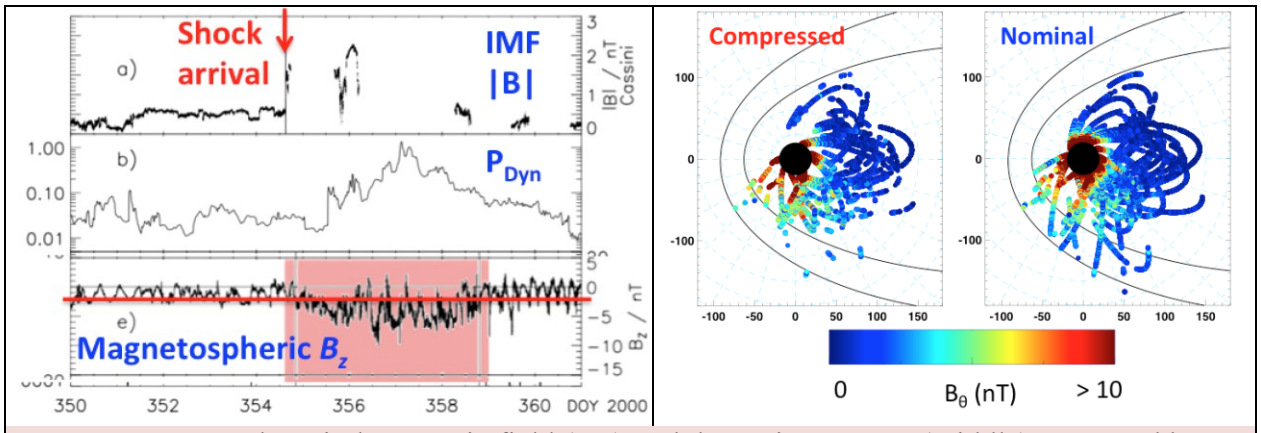

Figure 8. (left) Solar wind magnetic field (top) and dynamic pressure (middle) measured by Cassini upstream of Jupiter. (bottom) B_z measured by Galileo in the magnetosphere, compressed interval highlighted in red. Modified from Hanlon et al. (2004). **(right)** B_θ measurements during times of high (left) or low (right) solar wind dynamic pressure, inferred from a model. Black lines show the Joy et al. (2002) expanded and compressed magnetopause.

shifts shown in **Figure 1**. Vogt et al. (submitted) calculated the best fit current sheet current density index $\mu_0 I_0$ (Connerney et al., 1981, 1983), which roughly provides a measure of how distorted the magnetic field is from the planetary dipole, for each Galileo orbit. They found that changes in the magnetic field geometry were not consistent with concurrent latitudinal main emission shifts observed with HST, and concluded that the auroral shifts must be due in part to changes in other parts of the M-I coupling system, like the Pedersen conductivity or mass outflow rate from Io. We will expand on that preliminary analysis by examining the magnetic field for the 11 dates with concurrent HST images and classifying it as "weak", "average", or "strong". For each date we will then use the appropriate magnetic field fit to model the expected position and brightness of the main emission (using the model from Task B) for different values of $\Sigma_p^* / \dot{M}$. We will compare the predictions to concurrent HST observations. Identifying which values of $\Sigma_p^* / \dot{M}$ lead to agreement with the observations will place a constraint on these two quantities and how they vary during the Galileo era.

The outputs of the work in this task are the same as in Tasks A and B (model calculations of the local time dependence for quantities like plasma angular velocity, field-aligned currents and the resulting main emission mapping, etc.) but for two cases representing two temporal extremes ("weak" and "strong") for the magnetic field configuration. We will make predictions for the main emission brightness and position for the two cases. The physical significance of these results is that we will have quantified how *measured* temporal variabilities observed in Jupiter's magnetic field are expected to influence M-I coupling at Jupiter. Additionally, we will have used concurrent HST observations of the main auroral emission and Galileo measurements of the magnetic field to constrain Σ_p^* and $\dot{M}$ and their variability, which is a significant contribution because these quantities are difficult to measure. We will publish the results of this task as a paper in a peer-reviewed journal.

3. Research Team and Work Plan

PI Marissa Vogt will be responsible for the management of this investigation and compliance with all reporting requirements. PI Vogt will assist Co-I Khurana with the magnetic field analysis and current calculations described in Task A (steps 1 and 2), will perform the M-I coupling calculations described in Task A (step 3), and will perform the modeling work

described in Task B and C. PI Vogt will also be responsible for preparing manuscripts for publication, and implementation of the data management plan. Level of effort is 6 months per year. PI Vogt's research has focused on Jupiter's magnetosphere and aurora (Vogt et al., 2010, 2014a, 2015), including developing a Jovian M-I mapping model that includes local time asymmetries (Vogt et al., 2011). PI Vogt also has experience developing, testing, and implementing a computational model of Jupiter's magnetosphere (Vogt et al., 2014b).

Co-I Krishan Khurana will extend the analysis from his earlier study (Khurana, 2001) to the remaining Galileo orbits and will provide 2-D fits to all of the magnetic field data outside of the current sheet at Jupiter and will calculate the resulting currents as described in Task A (steps 1 and 2). He will assist with the M-I coupling calculations described in Task A (step 3) and the modeling working in Tasks B and C and will participate in the preparation of manuscripts describing our results. Effort is 1 month/year. Collaborator Khurana is one of the world's leading experts on modeling the Jovian magnetic field (e.g. Khurana, 1997) and he has extensive experience calculating currents and plasma properties from magnetic field data (e.g. Khurana and Kivelson, 1993; Khurana, 2001; Khurana and Schwarzl, 2005).

Collaborator Jonathan Nichols will advise on the modifications to the Nichols (2011) self-consistent magnetodisk model described in Task B and HST image analysis in Task C. Collaborator Nichols is one of the world's leading experts on M-I coupling at Jupiter. His research includes theoretical calculations (e.g. Nichols and Cowley, 2003), modeling (Nichols, 2011; Nichols et al., 2015), and analysis of HST auroral images (e.g. Nichols et al., 2007, 2009).

Collaborator Emma Bunce will advise on the calculation of currents and M-I coupling calculations in Task A. Collaborator Bunce is one of the world's leading experts on M-I coupling at Jupiter (e.g. Cowley and Bunce, 2001; Cowley and Bunce, 2003a, 2003b; Bunce et al., 2005).

Our work plan is as follows. Task A (years 1 and 2):

- Calculate 2-D fits to the magnetic field: Khurana 1 month (with Vogt and Bunce)
- Use the 2-D magnetic field fits to calculate currents: Khurana 1 month (w/Vogt and Bunce)
- Use the calculated currents to obtain 2-D functions of the plasma angular velocity and field-aligned currents; determine local time effects on the main emission: Vogt 2 months, with all
- Write up results of Task A and submit to peer-reviewed journal: Vogt 1.5 months, with all

Task B (years 1 and 2):

- Develop the modified magnetodisk model described in Task B, including testing and validation with simple magnetic field and reproducing Nichols (2011) published results: Vogt 4 months, with Nichols
- Run modified magnetodisk model described in Task B using magnetic field from Task A, run for range of values of $\Sigma_p^* / \dot{M}$: Vogt 3 months, with Nichols
- Write up results of Task B and submit to peer-reviewed journal: Vogt 1.5 months, with all

Task C (year 3):

- Calculate two extreme ("weak" and "strong") temporal fits to the magnetic field as described in Task C: Vogt 0.5 months, with Khurana 0.5 months
- Repeat the calculations from Tasks A and B above with the "weak" and "strong" temporal extreme magnetic field fits, plus comparison to HST images: Vogt 4 months, Khurana 0.5 months (Task A repeat), with Bunce and Nichols
- Write up results of Task C and submit to peer-reviewed journal: Vogt 1.5 months, with all

Note that time to write up results in each year for PI Vogt includes ~2 weeks to prepare for and attend professional meetings, at which intermediate results will be shared with the community.

References

Bagenal, F. and P. A. Delamere (2011), Flow of mass and energy in the magnetospheres of Jupiter and Saturn, *J. Geophys. Res.*, *116*, A05209, doi:10.1029/2010JA016294.

Bhardwaj, A., and G. R. Gladstone (2000), Auroral Emissions of the Giant Planets, *Rev. of Geophys.*, *38*, *3*, 295-353.

Bonfond, B., D. Grodent, J.-C. Gérard, T. Stallard, J. T. Clarke, M. Yoneda, A. Radioti, and J. Gustin (2012), Auroral evidence of Io's control over the magnetosphere of Jupiter, *Geophys. Res. Lett.*, *39*, L01105, doi:10.1029/2011GL050253.

Bonfond, B., J. Gustin, J.-C. Gérard, D. Grodent, A. Radioti, B. Palmaerts, S. V. Badman, K. K. Khurana, and C. Tao (2015), The far-ultraviolet main auroral emission at Jupiter – Part 1: Dawn–dusk brightness asymmetries, *Ann. Geophys*., *33*, 1203-1209, doi:10.5194/angeo-33-1203-2015.

Bunce, E. J. and S. W. H. Cowley (2001), Divergence of the equatorial current in the dawn sector of Jupiter's magnetosphere: analysis of Pioneer and Voyager magnetic field data, Planet. Space Sci., 49, 1089-1113, doi:10.1016/S0032-0633(01)00004-6.

Bunce, E. J., J. D. Nichols, and S. W. H. Cowley (2005), Solar wind-magnetosphere-ionosphere coupling at Jupiter, *Adv. Space Res., 36*, 2090–2099.

Caudal, G. (1986), A self-consistent model of Jupiter's magnetodisc including the effects of centrifugal force and pressure, *J. Geophys. Res.*, *91*(A4), 4201–4221, doi:10.1029/JA091ia04p04201.

Connerney, J., M. Acuña, and N. Ness (1981), Modeling the Jovian Current Sheet and Inner Magnetosphere, *J. Geophys. Res.*, *86*(A10), 8370-8384.

Connerney, J. E. P., M. H. Acuña, and N. F. Ness (1983), Currents in Saturn's magnetosphere, *J. Geophys. Res.*, *88*, 8779–8789.

Connerney, J. E. P., M. H. Acuña, N. F. Ness, and T. Satoh, (1998), New models of Jupiter's magnetic field constrained by the Io flux tube footprint, *J. Geophys. Res.*, *103*, 11929-11939.

Cowley, S. W. H., and E. J. Bunce (2001), Origin of the main auroral oval in Jupiter's coupled magnetosphere-ionosphere system, *Plan. Space Sci.*, *49*, 1067-1088.

Cowley, S. W. H., and E. J. Bunce (2003a), Modulation of Jovian middle magnetosphere currents and auroral precipitation by solar wind-induced compressions and expansions of the magnetosphere: initial response and steady state, *Planet. Space Sci.*, *51*, 31-56.

Cowley, S. W. H., and E. J. Bunce (2003b), Modulation of Jupiter's main auroral oval emissions by solar wind induced expansions and compressions of the magnetosphere, *Planet. Space Sci.*, *51*, 57-79.

Cowley, S. W. H., J. D. Nichols, and E. J. Bunce (2002), Distributions of current and auroral precipitation in Jupiter's middle magnetosphere computed from steady-state Hill-Pontius angular velocity profiles: Solutions for current sheet and dipole magnetic field models, *Planet. Space Sci*., *50*, 717.

Grodent, D., J. T. Clarke, J. Kim, J. H. Waite, and S. W. H. Cowley (2003), Jupiter's main auroral oval observed with HST-STIS, *J. Geophys. Res.*, 108, 1389, doi:10.1029/2003JA009921, A11.

Grodent, D., J.-C. Gérard, A. Radioti, B. Bonfond, and A. Saglam (2008), Jupiter's changing auroral location, *J. Geophys. Res.*, 113, A01206, doi:10.1029/2007JA012601.

Hanlon, P. G., M. K. Dougherty, N. Krupp, K. C. Hansen, F. J. Crary, D. T. Young, and G. Tóth (2004), Dual spacecraft observations of a compression event within the Jovian magnetosphere: Signatures of externally triggered supercorotation?, *J. Geophys. Res.*, 109, A09S09, doi:10.1029/2003JA010116.

Hess, S. L. G., B. Bonfond, P. Zarka, and D. Grodent (2011), Model of the Jovian magnetic field topology constrained by the Io auroral emissions, *J. Geophys. Res.*, *116*, A05217, doi:10.1029/2010JA016262.

Hill, T. W. (1979), Inertial Limit on Corotation, *J. Geophys. Res.*, *84*(A11), 6554-6558.

Hill, T. W. (2001), The Jovian auroral oval, *J. Geophys. Res.*, *106*, 8101-8107.

Khurana, K. K. (1997), Euler potential models of Jupiter's magnetospheric field, *J. Geophys. Res.*, *102*(A6), 11295-11306.

Khurana, K. K. (2001), Influence of solar wind of Jupiter's magnetosphere deduced from currents in the equatorial plane, *J. Geophys. Res.*, *106*, 25999.

Khurana, K. K., and M. G. Kivelson (1993), Inference of the angular velocity of plasma in the Jovian magnetosphere from the sweepback of magnetic field, *J. Geophys. Res.*, *98*, 67.

Khurana, K. K. and H. K. Schwarzl (2005), Global structure of Jupiter's magnetospheric current sheet, *J. Geophys. Res.*, *110*, doi:10.1029/2004JA010757.

Khurana, K. K., M. G. Kivelson, V. M. Vasyliūnas, N. Krupp, J. Woch, A. Lagg, B. H. Mauk, and W. S. Kurth (2004), The configuration of Jupiter's magnetosphere, in *Jupiter: the Planet, Satellites, and Magnetosphere*, edited by F. Bagenal et al., Cambridge Univ. Press, New York.

Kivelson, M. G., and K. K. Khurana (2002), Properties of the magnetic field in the Jovian magnetotail, *J. Geophys. Res.*, *107*(A8), 1196.

Krupp, N., A. Lagg, S. Livi, B. Wilken, J. Woch, E. Roelof, and D. Williams (2001), Global flows of energetic ions in Jupiter's equatorial plane: First-order approximation, *J. Geophys. Res.*, *106*(A11), 26017-26032.

Nichols, J. D. (2011), Magnetosphere-ionosphere coupling in Jupiter's middle magnetosphere: Computations including a self-consistent current sheet magnetic field model, *J. Geophys. Res., 116*, A10232, doi:10.1029/2011JA016922.

Nichols, J. D. (2011b), Magnetosphere ionosphere coupling at Jupiter like exoplanets with internal plasma sources: Implications for detectability of auroral radio emissions, *Mon. Not. R. Astron. Soc*., *414*, 2125–2138, doi:10.1111/j.1365-2966.2011.18528.x.

Nichols, J. D. (2012), Candidates for detecting exoplanetary radio emissions generated by magnetosphere—ionosphere coupling, *Mon. Not. R. Astron. Soc. Lett*., *427* (1): L75-L79. doi: 10.1111/j.1745-3933.2012.01348.x

Nichols, J. D., and S. W. H. Cowley (2003), Magnetosphere-ionosphere coupling currents in Jupiter’s middle magnetosphere: Dependence on the effective ionospheric Pedersen conductivity and iogenic plasma mass outflow rate, *Ann. Geophys*., *21*, 1419–1441.

Nichols, J. D., E. J. Bunce, J. T. Clarke, S. W. H. Cowley, J.-C. Gérard, D. Grodent, and W. R. Pryor (2007), Response of Jupiter's UV auroras to interplanetary conditions as observed by the Hubble Space Telescope during the Cassini flyby campaign, *J. Geophys. Res.*, 112, A02203, doi:10.1029/2006JA012005.

Nichols, J. D., J. T. Clarke, J. C. Gérard, and D. Grodent (2009), Observations of Jovian polar auroral filaments, *Geophys. Res. Lett., 36,* L08101, doi:10.1029/2009GL037578.

Nichols, J. D., N. Achilleos, and S. W. H. Cowley (2015), A model of force balance in Jupiter’s magnetodisc including hot plasma pressure anisotropy, *J. Geophys. Res. Space Physics*, *120*, 10,185–10,206, doi:10.1002/2015JA021807.

Pontius, D. H., Jr. (1997), Radial mass transport and rotational dynamics, *J. Geophys. Res.*, *102*(A4), 7137–7150, doi:10.1029/97JA00289.

Radioti, A., J.-C. Gérard, D. Grodent, B. Bonfond, N. Krupp, and J. Woch (2008), Discontinuity in Jupiter’s main auroral oval, *J. Geophys. Res.*, *113*, A01215, doi:10.1029/2007JA012610.

Ray, L. C., N. A. Achilleos, M. F. Vogt, and J. N. Yates (2014), Local time variations in Jupiter's magnetosphere-ionosphere coupling system, *J. Geophys. Res. Space Physics*, *119*, 4740–4751, doi:10.1002/2014JA019941.

Southwood, D. J., and M. G. Kivelson (2001), A new perspective concerning the influence of the solar wind on the Jovian magnetosphere, *J. Geophys. Res.*, 106*(A4)*, 6123-6130.

Tao, C., R. Kataoka, H. Fukunishi, Y. Takahashi, and T. Yokoyama (2005), Magnetic field variations in the Jovian magnetotail induced by solar wind dynamic pressure enhancements, *J. Geophys. Res.*, *110*, A11208, doi:10.1029/2004JA010959.

Vogt, M. F. (2012), The structure and dynamics of Jupiter's magnetosphere, Ph.D. thesis.

Vogt, M. F., M. G. Kivelson, K. K. Khurana, S. P. Joy, and R. J. Walker (2010), Reconnection and flows in the Jovian magnetotail as inferred from magnetometer observations, *J. Geophys. Res.*, *115,* A06219, doi: 10.1029/2009JA015098.

Vogt, M. F., M. G. Kivelson, K. K. Khurana, R. J. Walker, B. Bonfond, D. Grodent, and A. Radioti (2011), Improved mapping of Jupiter's auroral features to magnetospheric sources, *J. Geophys. Res., 116,* A03220, doi:10.1029/2010JA016148.

Vogt, M. F., C. M. Jackman, J. A. Slavin, E. J. Bunce, S. W. H. Cowley, M. G. Kivelson, and K. K. Khurana (2014a), Structure and Statistical Properties of Plasmoids in Jupiter's Magnetotail, *J. Geophys. Res. Space Physics*, *119*, 821-843, doi:10.1002/2013JA019393.

Vogt, M. F., M. G. Kivelson, K. K. Khurana, R. J. Walker, M. Ashour-Abdalla, and E. J. Bunce (2014b), Simulating the Effect of Centrifugal Forces in Jupiter's Magnetosphere, *J. Geophys. Res. Space Physics*, *119*, 1925-1950, doi:10.1002/2013JA019381.

Vogt, M. F., E. J. Bunce, M. G. Kivelson, K. K. Khurana, R. J. Walker, A. Radioti, B. Bonfond, and D. Grodent (2015), Magnetosphere-ionosphere mapping at Jupiter: Quantifying the effects of using different internal field models, *J. Geophys. Res. Space Physics*, *120*, 2584–2599, doi:10.1002/2014JA020729.

Vogt, M. F., E. J. Bunce, J. D. Nichols, J. T. Clarke, and W. S. Kurth, Long-term variability of Jupiter's magnetodisk and implications for the aurora, submitted to *J. Geophys. Res.* Feb. 2017, available for download at http://sites.bu.edu/marissavogt/files/2017/02/2017JA024066_Merged_PDF.pdf

Zieger , B. and K. C. Hansen (2008), Statistical validation of a solar wind propagation model from 1 to 10 AU, *J. Geophys. Res.*, 113, A08107, doi:10.1029/2008JA013046.